Top Catal (2015) 58:1159–1173
DOI 10.1007/s11244-015-0495-5

ORIGINAL PAPER

On the Structure Sensitivity of Dimethyl Ether Electro-oxidation on Eight FCC Metals: A First-Principles Study

Jeffrey A. Herron[1] · Peter Ferrin[1] · Manos Mavrikakis[1]

Published online: 24 September 2015

Abstract The electro-oxidation of dimethyl ether (DME) was investigated using periodic, self-consistent density functional theory (DFT) calculations on the (111) and (100) facets of eight fcc metals: Au, Ag, Cu, Pt, Pd, Ni, Ir, and Rh. The goal of this study is to understand the experimentally observed structure sensitivity of this reaction on Pt, and to predict trends in structure sensitivity of this reaction across the other seven metals studied. The main conclusion is that the enhanced activity of Pt(100) originates from more facile C–O bond breaking and removal of surface poisoning species, including CO and CH. When comparing C–O bond breaking energetics, we do not find a universal trend where these elementary steps are always more exergonic on the (100) facet. However, we find that, at a given potential, DME can be dehydrogenated (prior to breaking the C–O bond) to a greater extent on the (100) facet. Additionally, we find that the reaction energy for C–O bond breaking in CH_xOCH_y-type species becomes increasingly exergonic as the species becomes increasingly dehydrogenated. Together, the more facile dehydrogenation on the (100) facets provides more favorable routes to C–O bond activation. Though we calculate a lower onset potential on Au(100), Ag(100), Cu(100), Pt(100), and Pd(100) than their respective (111) facets, the calculated onset potential for Ni(100), Ir(100), and Rh(100) are actually higher than for their respective (111) facets. Finally, by constructing theoretical volcano plots, we conclude that Au(100), Ag(100), Cu(100), Pt(100), and Pd(100) should be more active than their respective (111) facets, while Ni(100), Rh(100), and Ir(100) will show the opposite trend.

Keywords Density functional theory · Heterogeneous catalysis · Thermochemistry · Electrocatalysis · Oxidation · Dimethyl ether

1 Introduction

Dimethyl ether (DME) is a promising alternative fuel [1, 2], which has been suggested as a viable liquid-phase feed for low-temperature polymer electrolyte membrane (PEM) fuel cells [3, 4–8]. DME used as a fuel for fuel cells can alleviate some of the serious drawbacks to other promising liquid fuels, including methanol and ethanol. Methanol crossover to the cathode reduces the efficiency of direct methanol fuel cells [9, 10], and the reduced dipole moment of DME has shown to reduce DME crossover to the cathode [11]. Furthermore, the C–C bond in ethanol is difficult to break, which makes complete oxidation to CO_2 difficult [3, 12]. Though there is significant interest in using DME as a fuel for fuel cells, the reaction mechanism is poorly understood. As a result, researchers have been ill-equipped for finding electrocatalysts with sufficient activity, high efficiency and low cost [3]. Notably, researchers have explored Pt-based catalysts such as PtRu, which are highly active for methanol electro-oxidation [13]. However, these have shown inferior activity to pure Pt for this reaction [13].

In order to provide insight into the DME electro-oxidation reaction mechanism, researchers have studied the

Electronic supplementary material The online version of this article (doi:10.1007/s11244-015-0495-5) contains supplementary material, which is available to authorized users.

✉ Manos Mavrikakis
emavrikakis@wisc.edu

[1] Department of Chemical and Biological Engineering, University of Wisconsin – Madison, Madison, WI 53706, USA

reaction on single-crystal Pt electrodes [14–16]. Interestingly, they have found a remarkable structure sensitivity for this reaction [14–17]. In particular, Pt(100) is significantly more active than Pt(111) [16]. The main anodic oxidation peak at 0.8 V versus the reversible hydrogen electrode (RHE) is approximately 30 times larger on Pt(100) than on Pt(111) [16]. This improved activity has been attributed to the more facile C–O bond breaking on the (100) facet of Pt [16]. Lu et al. synthesized Pt nanocubes with preferential (100) surfaces that showed approximately three times the activity of commercial Pt black, again demonstrating this structure sensitivity [18].

With the goal of identifying improved catalysts for this reaction, here we report a first-principles, density functional theory analysis into the mechanism of dimethyl ether electro-oxidation on late transition metals. In this paper, we specifically address the origins of the structure sensitivity of this reaction. Previously, we investigated the reaction mechanism for dimethyl ether electro-oxidation on close-packed facets of late transition metals [19]. Here, we explore the possible reasons why Pt(100) is much more active than Pt(111) for this reaction. Then, we extend our analysis to other model, monometallic (Au, Ag, Cu, Pt, Pd, Ni, Ir, Rh) fcc(111) and fcc(100) surfaces to provide further insight into the nature of the structure sensitivity. Some of these surfaces may be of interest as DME electro-oxidation catalysts either as pure metals (if metallic under electro-oxidation conditions) or as a component of multi-metallic catalysts.

2 Methods

The free energies of reaction species are calculated using spin-polarized, self-consistent density functional theory, as implemented in the DACAPO [20, 21] total energy code. Calculations are performed on the (111) and (100) facets of selected face-centered cubic (fcc) metals: Rh, Ir, Ni, Pd, Pt, Cu, Ag, and Au. The (111) surfaces are represented using a periodic 3 × 3 unit cell with three layers of metal atoms that are fixed at their optimized bulk positions. Previous calculations have shown that relaxation effects on these close-packed surfaces are minimal [22–25]. The (100) surfaces are modeled using a periodic 3 × 3 unit cell with four layers of metal atoms. The atoms in the top two layers of the (100) slabs are fully relaxed, while the bottom two layers are fixed at their optimized bulk positions. At least five equivalent layers of vacuum separate successive slabs in the z-direction. The lattice constants for these metals were optimized. The optimized bulk lattice constants (experimental value [26] in parentheses) are Ag 4.14 Å (4.09 Å), Au 4.18 Å (4.08 Å), Cu 3.67 Å (3.62 Å), Ir 3.86 Å (3.83 Å), Ni 3.52 Å (3.52 Å), Pd 3.99 Å (3.89 Å), Pt 4.00 Å (3.92 Å), Rh 3.83 Å (3.80 Å). Adsorption is permitted on only one of the two exposed surfaces, and the dipole moment is adjusted accordingly [27, 28]. The ionic cores are described using ultrasoft Vanderbilt pseudopotentials [29]. The Kohn–Sham one-electron states are expanded in a series of plane waves with an energy cutoff of 25 Ry. Based on convergence tests, the surface Brillouin zone of the (111) facets are sampled with 18 special Chadi–Cohen [30] k-points and the (100) facets are sampled with a 4 × 4 × 1 Monkhorst–Pack [31] k-point mesh. The exchange–correlation energy and potential are calculated self-consistently using the PW91 generalized-gradient approximation [32]. The electron density is determined by iterative diagonalization of the Kohn–Sham Hamiltonian, Fermi population of the Kohn–Sham states ($k_BT = 0.1$ eV), and the Pulay mixing of the resulting electronic density. All total energies are extrapolated to $k_BT = 0$ eV.

The zero-point energy (ZPE) is included in the calculation of the free energy of all adsorbates. The zero-point energies are calculated assuming a quantum harmonic oscillator with calculated vibrational frequencies. The vibrational frequencies are calculated by numerical differentiation of forces using a second-order finite difference approach with a step-size of 0.015 Å [33]. The Hessian matrix is mass-weighted and diagonalized to yield the frequencies and normal modes of the adsorbed species. For surface adsorbates, the vibrational frequencies were only evaluated on Pt(111) and Pt(100), and were assumed (as a first approximation) to be the same on other surfaces with the same crystal structure due to similar adsorption geometries. The entropy of all surface species is calculated including translation, vibration, and rotation.

Calculations of free energy are done relative to DFT-derived energies of $H_2O(g)$, $CO_2(g)$, and $H_2(g)$. For example, the free energy of dimethyl ether is calculated from the reaction: $2CO_2(g) + 6H_2(g) \rightarrow 3H_2O(l) + CH_3OCH_3(g)$, which leads to:

$$\begin{aligned}\Delta G_{CH_3OCH_3} = &(E_{CH_3OCH_3} - TS_{CH_3OCH_3} + Z_{CH_3OCH_3}) \\ &+ 3(E_{H_2O} - TS_{H_2O} + Z_{H_2O}) \\ &- 2(E_{CO_2} - TS_{CO_2} + Z_{CO_2}) \\ &- 6(E_{H_2} - TS_{H_2} + Z_{H_2})\end{aligned}$$

where E_i is the total energy of a species i calculated from DFT, T is the absolute temperature (298 K), S_i is the calculated entropy and Z_i is the calculated zero-point energy for the species. The calculation of free energies of other species is done similarly. When calculating the free energy of surface species, the total energy of the species is taken relative to the clean surface, while the entropy and zero-point energy are calculated for the adsorbed state. Using this approach, we calculate free energies of formation for gas phase CH_3OCH_3, CH_3OH, and HCOOH as 0.39, 0.11, and 0.42 eV, respectively. The corresponding experimental

values are −0.09, 0.04, and 0.34 eV, respectively [26]. We note that there are well known difficulties for the GGA-PW91 functional for describing these gas phase energetics, though we do not expect these discrepancies to affect the overall results of our analysis.

To correct the calculated free energy for the electrochemical potential, we employ a simple procedure which has previously been applied to studies of oxygen evolution [34, 35], oxygen reduction [36, 37], methanol oxidation [22, 23] and ammonia oxidation [38] at electrode surfaces. First, we choose the reversible hydrogen electrode as a reference. At standard conditions, hydrogen gas is in equilibrium with protons and electrons, at a defined potential of 0 V. A change in the electrode potential by U will shift the free energy of the electrons exergonically by $|e|U$, where $|e|$ is the absolute charge of an electron. Therefore, if we consider the first dehydrogenation of dimethyl ether step: $CH_3OCH_3(g) + * \rightarrow CH_2OCH_3* + H^+ + e^-$, a change in the potential by U will adjust the free energy change of this reaction by $-|e|U$.

Activation energy barriers are not calculated for any of the reaction steps studied. Studies of Brønsted–Evans–Polanyi (BEP) relationships suggest a strong correlation between the thermochemistry of reaction steps and their kinetics and for the purpose of this study we rely on the reaction thermochemistry alone [39, 40]. The existence of C–O bond breaking events does complicate the analysis, as these barriers are not necessarily a function of the electrode potential. Furthermore, the thermochemistry is calculated at 1/9 ML surface coverages. The surface coverages of various intermediates under electrochemical oxidation conditions may be different, and this could contribute to differences between experiments and these calculations [33, 41–45]. Also, we neglect any contributions from solvation on binding energies of adsorbed species [46–49]. We note that past DFT studies have calculated that solvation stabilizes OH, which is adsorbed on Pt(111), by ~0.5 eV, and this may affect the overall conclusions [36, 37, 50]. However, it is likely that other adsorbates in the reaction, perhaps especially those with an –OH group, may be stabilized to a similar extent. Therefore, as we (or others in the literature [51, 52]) have not performed systematic studies of solvation on all of the adsorbates, we omit those effects from our analysis so as not to unfairly bias the results. Nevertheless, we proceed with these limitations of our model in mind.

3 Results and Discussion

In Scheme 1 we present the DME electro-oxidation network that is considered in this study. The reaction begins with proton/electron transfer from DME to yield a CH_xOCH_y intermediate (x, y = 0, 1, 2, or 3). Then, the C–O bond of this CH_xOCH_y intermediate is broken to yield CH_x and OCH_y species. Finally, these species are oxidized to CO_2. There are many different routes for DME to be oxidized to CO_2, and each surface studied may have its own unique pathway.

The energetics of the elementary steps shown in Scheme 1 are calculated from the free energies of the individual species, as described in the methods section. The calculated free energies of the individual species at 298 K and 0 V are listed in Table 1. From the free energies we see that, for most cases, a particular intermediate is more stable on the (100) facet than the (111) facet of a given metal. This is true for all species studied on Au, Cu, Pt, Ir, and Rh. Pd is a notable exception where several intermediates are more stable on the (111) facet.

We begin our analysis by trying to explain the experimental observation that the electro-oxidation activity is much higher on Pt(100) when compared with Pt(111) [14–16, 18]. Our analysis shows that there are two key reasons for this behavior: (1) C–O bond activation is easier on Pt(100) than Pt(111) and (2) the oxidation (i.e. removal) of surface poisons (for Pt, CO and CH) that are formed after C–O bond breaking is also easier on Pt(100) than Pt(111). Then, we will extend our analysis to (111) and (100) surfaces of other elemental fcc metals, namely: Au, Ag, Cu, Pd, Ni, Ir, and Rh.

3.1 C–O Bond Activation on Pt(111) and Pt(100)

In Scheme 2 we show the free energies of reaction for proton/electron transfer and C–O bond breaking events on Pt(111) and Pt(100) at 0 V. Experiments and theory have demonstrated that under-coordinated sites are more active than close-packed surfaces for bond-breaking in a number of systems including CO [53–55], N_2 [56, 57], and NO [58, 59]. It has been suggested that, in general, dissociation reactions are always favored over defects than on flat terraces [60]. Therefore, one might hypothesize that C–O bond breaking in DME is easier on more-open, flat surfaces when compared with close-packed surfaces. However, we note that only eleven of the sixteen possible C–O bond breaking events are more exergonic on Pt(100) than on Pt(111). Furthermore, only six of the eleven possible proton/electron transfer steps are more exergonic on Pt(100) than on Pt(111). Why is this? Earlier, we noted that all of the intermediates are more stable on Pt(100) than Pt(111). Therefore, for elementary steps where the initial state and final state species are all bound to the surface (no vapor phase species involved), the energy of the initial and final states will both be lower in energy (more negative) on the (100) facet than on the (111) facet. However, the two states are not stabilized equally because some intermediates are

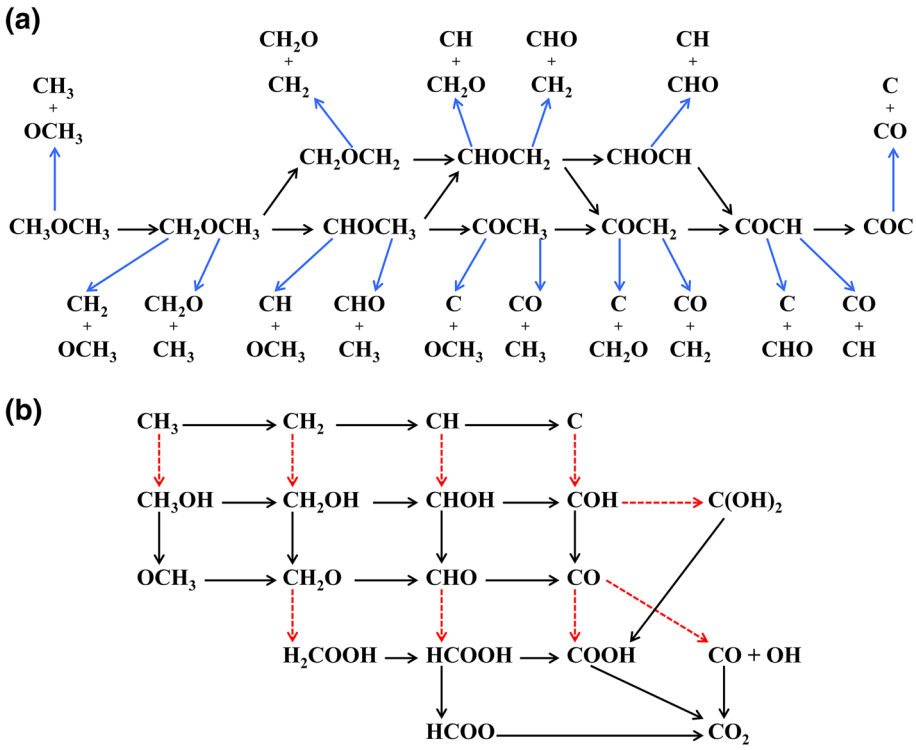

Scheme 1 Reaction network for DME electro-oxidation. **a** Proton/electron transfer from COC backbone and C–O bond breaking. **b** Electro-oxidation of intermediates derived from DME through C–O bond breaking. Proton/electron transfer steps shown with black arrows, C–O bond breaking steps shown with *blue arrows*, and Heyrovsky type reactions (involving H_2O activation) shown with *dotted red arrows*. Reaction stoichiometry is balanced with H_2O, H^+ and e^- species

much more stabilized on the (100) facet than others. For example, $CHOCH_3$ is 0.52 eV more stable on Pt(100) while $COCH_3$ is only 0.03 eV more stable on Pt(100), when compared with Pt(111). As a result, these bond-breaking events are not always more exergonic on Pt(100) than Pt(111). The same conclusion can be drawn for other metals studied here. We do caution, however, that this analysis is only based on reaction thermochemistry. Following a hypothetical, reaction-independent BEP correlation [40], we would expect a lower activation energy barrier for an elementary step with a more negative reaction energy.

Since the reaction energy of these elementary steps are not always more exergonic on Pt(100) as compared to Pt(111), the analysis of the structure sensitivity must be more elaborate. We analyze the data with a few simple assumptions: (1) if the free energy of reaction of a proton/electron transfer is exergonic, then it can proceed. Otherwise, if it is endergonic, then the step cannot occur. (In principle, there can be flux through proton/electron transfer steps even if the step is endergonic, but the flux is assumed to be low) [61]. (2) The difficulty of all the C–O bond-breaking steps is correlated with their reaction energies through a universal BEP correlation. Therefore, if we compare two C–O bond breaking events, then the one that is more exergonic will have a lower activation energy barrier than the other.

At 0 V, proton/electron transfer from DME is endergonic on Pt(100) and Pt(111) (see Scheme 2). Therefore, the only option available is to break the C–O bond to form CH_3 and OCH_3. The free energy of C-O bond-breaking is 0.50 eV on Pt(111) and −0.03 eV on Pt(100). Therefore, we would expect C–O bond breaking to be easier on Pt(100) at 0 V.

If the potential were increased, the free energy of reaction for proton/electron transfer steps (dehydrogenation) becomes more exergonic, allowing for the formation of other intermediates prior to breaking the C–O bond. Would this affect the conclusion of whether Pt(100) or Pt(111) is more active? First, let us consider how the energetics of C–O bond breaking change as DME is dehydrogenated. Consider the dehydrogenation pathway: $CH_3OCH_3 \rightarrow CH_2OCH_3 \rightarrow CHOCH_3 \rightarrow COCH_3 \rightarrow COCH_2 \rightarrow COCH \rightarrow COC$. For most of these species, there are two possible C–O bond scission reactions (e.g., $CH_2OCH_3 \rightarrow CH_2 + OCH_3$, $\Delta G_{Pt(111)} = 0.64$ eV or $CH_2OCH_3 \rightarrow CH_2O + CH_3$, $\Delta G_{Pt(111)} = -0.13$ eV), and we will consider only the more exergonic of these (as we assume that step to have a lower activation energy). For Pt(111), the free energies of reaction for breaking the C–O bond in these species can be ranked as: CH_3OCH_3 (0.50 eV) > CH_2OCH_3 (−0.13 eV) > $CHOCH_3$ (−0.72 eV) > $COCH_3$ (−0.81 eV) > $COCH_2$ (−1.33 eV) > COCH (−2.70 eV) > COC (−2.81 eV). That is, the reaction energy becomes more exergonic for every successive dehydrogenation. We see the same result on Pt(100): CH_3OCH_3(−0.03 eV) > CH_2OCH_3(−0.10 eV) > $CHOCH_3$(−0.49 eV) > $COCH_3$ (−1.24 eV) > $COCH_2$(−1.71 eV) > COCH(−2.27 eV) >COC −3.19 eV). Note, this trend does not always hold if a different dehydrogenation pathway is considered.

Table 1 Free energies of adsorbed species at 298 K and 0 V for each surface studied

	Free energies (eV)															
	Au		Ag		Cu		Pt		Pd		Ni		Ir		Rh	
	(111)	(100)	(111)	(100)	(111)	(100)	(111)	(100)	(111)	(100)	(111)	(100)	(111)	(100)	(111)	(100)
CH_2OCH_3	1.45	**1.25**	1.82	**1.73**	1.65	**1.46**	0.59	**0.41**	0.81	0.81	1.10	**0.81**	0.60	**0.46**	0.70	**0.64**
CH_2OCH_2	2.20	**1.88**	2.70	**2.56**	2.46	**2.03**	0.56	**0.42**	**1.07**	1.09	1.53	**0.78**	0.65	**0.11**	0.88	**0.46**
$CHOCH_3$	2.35	**1.81**	2.68	**2.44**	2.16	**1.85**	0.84	**0.32**	0.94	**0.76**	1.05	**0.75**	0.59	**0.18**	0.72	**0.41**
$CHOCH_2$	2.68	**2.42**	**3.20**	3.21	2.49	**2.28**	0.34	**0.23**	**0.88**	1.09	**1.18**	1.23	0.24	**−0.07**	0.61	**0.21**
$COCH_3$	2.59	**2.27**	3.03	**2.88**	2.04	**1.69**	0.14	**0.11**	**0.33**	0.39	**0.41**	0.74	0.09	**−0.30**	0.10	**0.03**
$COCH_2$	4.13	**3.23**	4.60	**4.17**	4.07	**2.80**	1.00	**0.53**	**1.33**	1.47	1.42	**0.86**	0.78	**0.02**	0.79	**0.43**
CHOCH	3.92	**2.86**	4.41	**3.71**	3.46	**2.72**	1.06	**−0.08**	1.88	**0.95**	1.77	**0.76**	0.61	**−0.57**	1.06	**−0.02**
COCH	5.39	**4.34**	5.82	**4.97**	4.35	**3.92**	2.06	**1.17**	**2.26**	2.37	2.36	**1.70**	1.39	**0.33**	1.46	**0.83**
COC	6.02	**5.63**	5.59	**4.72**	4.52	**3.79**	3.13	**2.30**	**3.22**	3.45	2.63	**2.44**	2.56	**1.15**	2.24	**1.61**
CH_3O	1.76	**1.32**	0.98	**0.70**	0.52	**0.29**	1.14	**0.71**	0.93	**0.83**	0.23	**0.04**	0.65	**0.02**	0.30	**0.18**
CH_3	0.55	**0.38**	0.80	**0.73**	0.43	**0.33**	−0.25	**−0.35**	**0.00**	0.07	**−0.11**	−0.10	−0.17	**−0.44**	−0.16	**−0.34**
CH_2OH	1.36	**1.18**	1.76	**1.64**	1.56	**1.26**	0.42	**0.31**	0.66	**0.63**	1.04	**0.60**	0.61	**0.03**	0.52	**0.27**
CH_2	1.65	**1.10**	1.93	**1.81**	1.30	**1.18**	0.09	**−0.40**	0.33	**0.30**	0.15	**0.13**	−0.01	**−0.59**	0.06	**−0.25**
CHOH	2.14	**1.46**	2.54	**2.17**	1.96	**1.57**	0.53	**−0.18**	0.71	**0.29**	0.87	**0.45**	0.16	**−0.30**	0.66	**−0.01**
CHO	1.49	**1.30**	1.84	**1.71**	1.54	**1.21**	0.37	**0.18**	0.36	**0.29**	0.49	**0.27**	0.22	**−0.66**	0.16	**−0.60**
CH	2.22	**1.92**	2.75	**2.21**	1.68	**0.91**	−0.22	**−0.32**	0.19	**−0.09**	0.09	**−0.51**	−0.40	**−1.05**	−0.29	**−0.93**
COH	2.59	**1.58**	3.06	**2.76**	2.04	**1.56**	0.07	**−0.08**	0.25	**0.04**	0.33	**−0.12**	−0.01	**−0.59**	−0.01	**−0.55**
CO	1.19	**0.72**	1.24	**1.02**	0.61	**0.50**	−0.42	**−0.78**	−0.66	**−0.62**	−0.52	**−0.71**	−0.55	**−1.05**	−0.59	**−0.90**
C	3.63	**2.84**	4.15	**3.11**	3.01	**1.49**	0.74	**−0.12**	0.84	**−0.30**	0.92	**−0.67**	0.43	**−0.76**	0.26	**−0.99**
HCOO	1.28	**1.07**	0.73	**0.50**	0.44	**0.12**	0.76	**0.61**	**0.63**	0.65	1.05	**−0.08**	0.09	**−0.14**	0.02	**−0.06**
COOH	1.42	**1.34**	1.56	**1.45**	1.22	**1.01**	0.39	**0.17**	0.49	**0.4**	0.48	**0.28**	0.08	**−0.32**	0.10	**−0.19**
$C(OH)_2$	1.56	**1.37**	1.98	**1.92**	1.64	**1.45**	0.14	**−0.04**	0.65	**0.26**	0.92	**0.56**	0.25	**−0.27**	0.46	**0.14**
H_2COOH	2.13	**1.48**	1.54	**0.96**	1.14	**0.52**	1.48	**0.96**	1.45	**0.97**	0.85	**0.21**	1.14	**0.27**	0.79	**0.25**
OH	1.71	**1.10**	0.98	**0.53**	0.57	**0.17**	1.16	**0.56**	1.04	**0.7**	0.29	**−0.04**	0.67	**−0.08**	0.54	**0.02**

All values are in eV. For each metal, the facet on which each intermediate is more stable, is noted in bold font. Free energies of closed-shell species are: CH_3OCH_3 (0.39 eV), CH_3OH (0.11 eV), HCOOH (0.42 eV), and CH_2O (0.71 eV)

These results show that C–O bond breaking becomes easier on both Pt(111) and Pt(100) as DME is dehydrogenated. Furthermore, the degree to which DME can be dehydrogenated depends upon the potential of the electrode (as this affects proton/electron transfer steps energetics). Therefore, as the potential increases, C–O bond breaking becomes easier because a more dehydrogenated CH_xOCH_y species can form. However, to determine whether Pt(111) or Pt(100) is more active for C–O bond breaking, we need to compare the C–O bond breaking energy as a function of potential. Following the same analysis as before, we demonstrate the results on Pt(111) at 0.20 and 0.25 V in Scheme 3. At 0.20 V, it becomes thermoneutral to remove the first hydrogen from DME to form CH_2OCH_3. Subsequent proton/electron extractions to form CH_2OCH_2 and $CHOCH_2$ are also exergonic at this potential. Therefore, at 0.20 V, C–O bond breaking can occur (with free energy of reaction for the more exergonic of the two possible C–O bond breaking events per intermediate given in parentheses) for CH_3OCH_3 (0.50 eV), CH_2OCH_3 (−0.13 eV), CH_2OCH_2 (0.24 eV), and $CHOCH_2$ (0.12 eV). The C–O bond breaking event: $CH_2OCH_3 \rightarrow CH_2O + CH_3$ has the most exergonic reaction energy of these, and we use this value as a measure of the difficulty of breaking the C–O bond at this potential. At 0.25 V, additional proton/electron transfer steps become exergonic, opening additional pathways. It is possible to form $CHOCH_3$ and $COCH_3$, with C–O bond breaking energies of −0.72 and −0.81 eV, respectively. The most exergonic C–O bond breaking step at this potential is via $COCH_3$, with a value of −0.81 eV.

We obtain the results shown in Fig. 1 by performing this analysis from 0 to 1.2 V on Pt(111) and Pt(100). From these results, we see that C–O bond breaking is more exergonic on Pt(100) than on Pt(111) from 0 to 0.99 V and above 1.13 V. (We note that above 1.13 V, DME can be fully dehydrogenated to COC on both surfaces, and so there will not be a change in the C–O bond breaking step above this potential.) C–O bond breaking is more exergonic on Pt(111) between 0.99 and 1.13 V. At the oxidation peak potential for Pt(111) and Pt(100), approximately 0.80 V [14, 15], C–O bond breaking should be easier on Pt(100) than on Pt(111), in agreement with the experimental hypothesis [14–16]. At this potential, DME can be dehydrogenated to $COCH_2$ prior to breaking the C–O bond

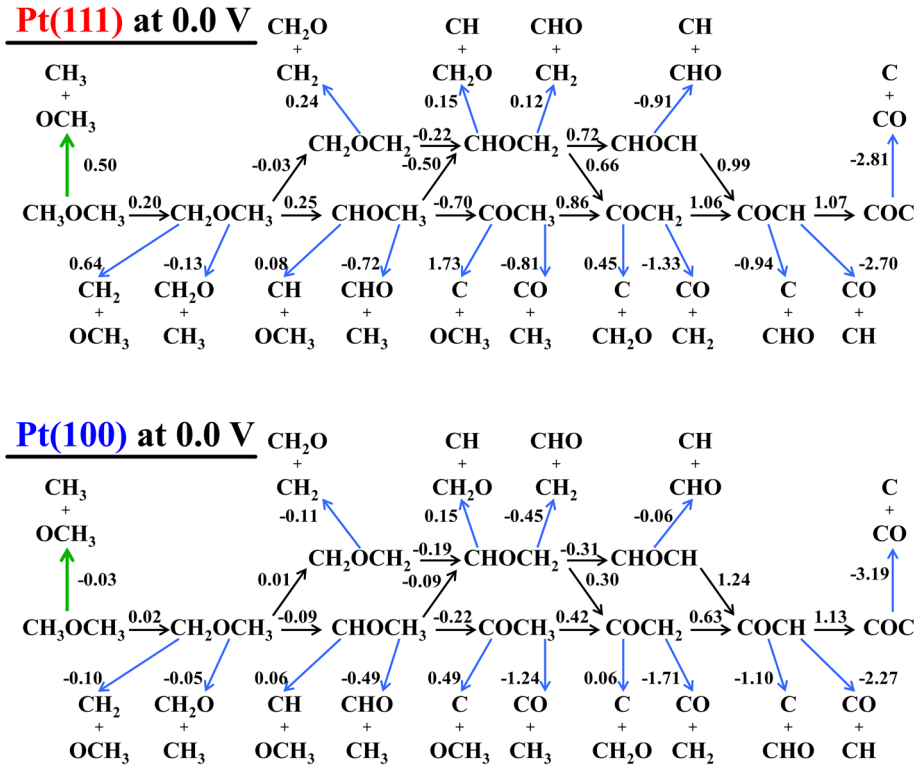

Scheme 2 Free energies of reaction on Pt(111) and Pt(100) for proton/electron transfer steps and C–O bond breaking of DME backbone at 0 V. In *black arrows* are proton/electron transfer steps, and in *blue arrows* are C–O bond breaking steps. The *green arrows* show the active pathway at 0 V. Reaction stoichiometry is balanced with H_2O, H^+ and e^- species

on Pt(111). On Pt(100), DME can be dehydrogenated to COCH, in agreement with a previous combined experimental and DFT study [62, 63]. The free energies of these C–O bond breaking reactions are −1.33 and −2.27 eV, respectively.

3.2 Oxidation of CH_x and OCH_y Fragments on Pt(111) and Pt(100)

Once the C–O bond of DME (or dehydrogenated DME, CH_xOCH_y) is broken, the resulting CH_x and OCH_y fragments must be oxidized to CO_2. Though we refer to the C–O bond scission products generally as CH_x and OCH_y, they could otherwise be referred to as CH_xO and CH_y. For example, CH_2OCH_3 could otherwise be referred to as CH_3OCH_2, and C–O bond breaking of either species has the possible products of $CH_2 + OCH_3$ and $CH_3 + OCH_2$. The energetics of the possible elementary steps involved on Pt(111) and Pt(100) are shown in Scheme 4. To predict the active oxidation pathway, we follow a simple, systematic approach. At each junction in the network, we follow the most exergonic elementary step that is available. The underlying assumption is that there exists a universal BEP correlation for these electrochemical steps and therefore when comparing two electrochemical steps, the one with the more negative reaction energy will have a lower activation energy barrier. First, we discuss our prediction for the oxidation pathway on Pt(111) and Pt(100) at 0 V. Then, we discuss how changing the potential would affect the pathway.

On Pt(111), at 0 V, DME is dissociated directly to CH_3 and OCH_3. These two fragments must be oxidized to CO_2. First we examine the oxidation of CH_3 to CO_2. The calculated pathway is $CH_3 \rightarrow CH_2 \rightarrow CH \rightarrow CHOH \rightarrow COH \rightarrow CO \rightarrow COOH \rightarrow CO_2$ and the details of this result follow. CH_3 can be oxidized to CH_2 ($\Delta G = 0.34$ eV) or CH_3OH ($\Delta G = 0.36$ eV). The former is slightly more driven so we assume that CH_2 is formed. CH_2 can be oxidized to CH ($\Delta G = -0.31$ eV) or CH_2OH ($\Delta G = 0.33$ eV). Oxidation to CH is strongly favored. CH is oxidized to C ($\Delta G = 0.96$ eV) or CHOH ($\Delta G = 0.74$ eV). CHOH is more stable. CHOH can be oxidized to COH ($\Delta G = -0.46$ eV) or CHO ($\Delta G = -0.15$ eV), with the COH pathway more favorable. COH is then oxidized to CO ($\Delta G = -0.49$ eV) rather than to $C(OH)_2$ ($\Delta G = 0.07$ eV). Finally, CO is oxidized to COOH ($\Delta G = 0.81$ eV) and then CO_2 ($\Delta G = -0.39$ eV).

The OCH_3 fragment is oxidized along the following pathway on Pt(111) at 0 V: $OCH_3 \rightarrow CH_2O \rightarrow CHO \rightarrow CO \rightarrow COOH \rightarrow CO_2$. First OCH_3 is oxidized to CH_2O ($\Delta G = -0.43$ eV), which can be oxidized to H_2COOH ($\Delta G = 0.77$ eV) or CHO ($\Delta G = -0.34$ eV). CHO formation is favored. Then CHO can be oxidized to CO ($\Delta G = -0.80$ eV) or HCOOH ($\Delta G = 0.05$ eV). CO is strongly favored, which is then oxidized to CO_2 as previously described.

Scheme 3 C–O bond breaking pathways on Pt(111) as a function of potential. Values listed are free energies of reaction (in eV) at a given potential. In *black* arrows are proton/electron transfer steps, and in *blue* arrows are C–O bond breaking steps. The *red* arrows show pathways that are available at the given potential. The *green* arrow shows the most exergonic C–O bond breaking step that is possible at the given potential. Reaction stoichiometry is balanced with H_2O, H^+ and e^- species

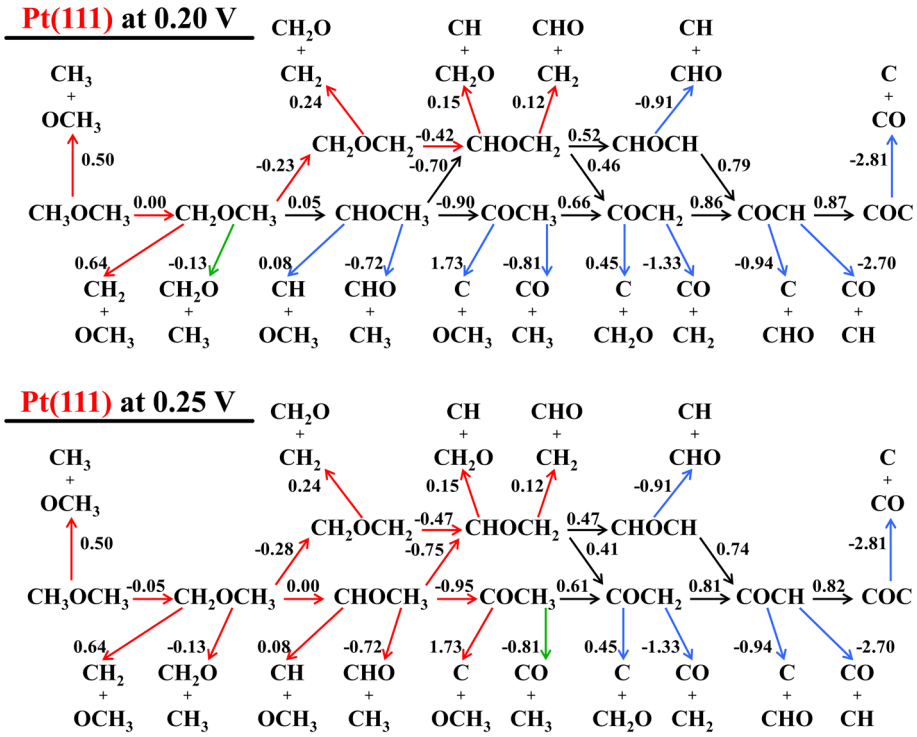

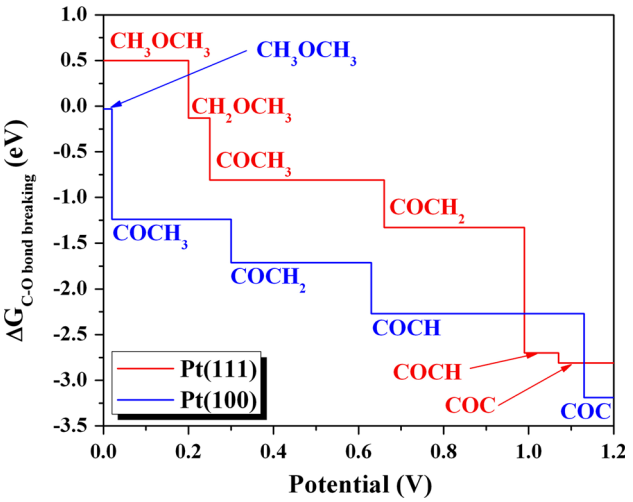

Fig. 1 Reaction energy of the most exergonic C–O bond breaking step possible at a given potential on Pt(111) and Pt(100). The labels correspond to the species that is able to form at a given potential which can be dissociated with the most exergonic reaction energy

From these results we see that on Pt(111), oxidizing OCH_3 to CO involves only exergonic steps at 0 V, while CH_3 to CO involves several endergonic elementary steps. Of these, oxidizing CH to CHOH is the most difficult ($\Delta G = 0.74$ eV). However, the overall most difficult electrochemical step in the oxidation reaction is oxidizing CO to COOH ($\Delta G = 0.81$ eV), which is required to oxidize both CH_3 and OCH_3 to CO_2. Therefore, we would predict an onset potential for oxidation when this particular elementary step becomes exergonic. This would occur at 0.81 V. We note that experiments have demonstrated that CO oxidation on Pt(111) occurs at step sites [64], and therefore the experimentally measured onset potential may be lower than what is suggested by this analysis. However, as the next most difficult step requires an onset potential of 0.74 V (CH oxidation), the overall onset potential would not change significantly.

Now, we contrast these results with Pt(100). At 0 V, DME will dissociate to CH_3 and OCH_3. The calculated oxidation pathway for CH_3 is: $CH_3 \rightarrow CH_2 \rightarrow CH \rightarrow CHOH \rightarrow COH \rightarrow CO \rightarrow CO + OH \rightarrow CO_2$, and the pathway for OCH_3 is: $OCH_3 \rightarrow CH_2O \rightarrow CHO \rightarrow CO \rightarrow CO + OH \rightarrow CO_2$. This pathway is the same as on Pt(111) up to CO formation. After CO formation on Pt(100), CO can be oxidized to CO_2 by reacting with coadsorbed OH species, rather than by forming a COOH intermediate. For CH_3 oxidation to CO, the most difficult step is the same as on Pt(111), CH → CHOH. However, in this case, the reaction is only slightly endergonic ($\Delta G = 0.14$ eV). Again, like Pt(111), oxidation of OCH_3 to CO is exergonic for all elementary steps. Overall, the most difficult step in the oxidation mechanism is activation of water ($\Delta G = 0.56$ eV) in order to provide OH for oxidation of CO to CO_2. Therefore, on Pt(100) the predicted onset potential is 0.56 V.

When we compare the oxidation of these fragments at 0 V between Pt(111) and Pt(100), we see that the majority of the oxidation pathway is the same. The main difference is in the reaction step used to remove CO, which is the

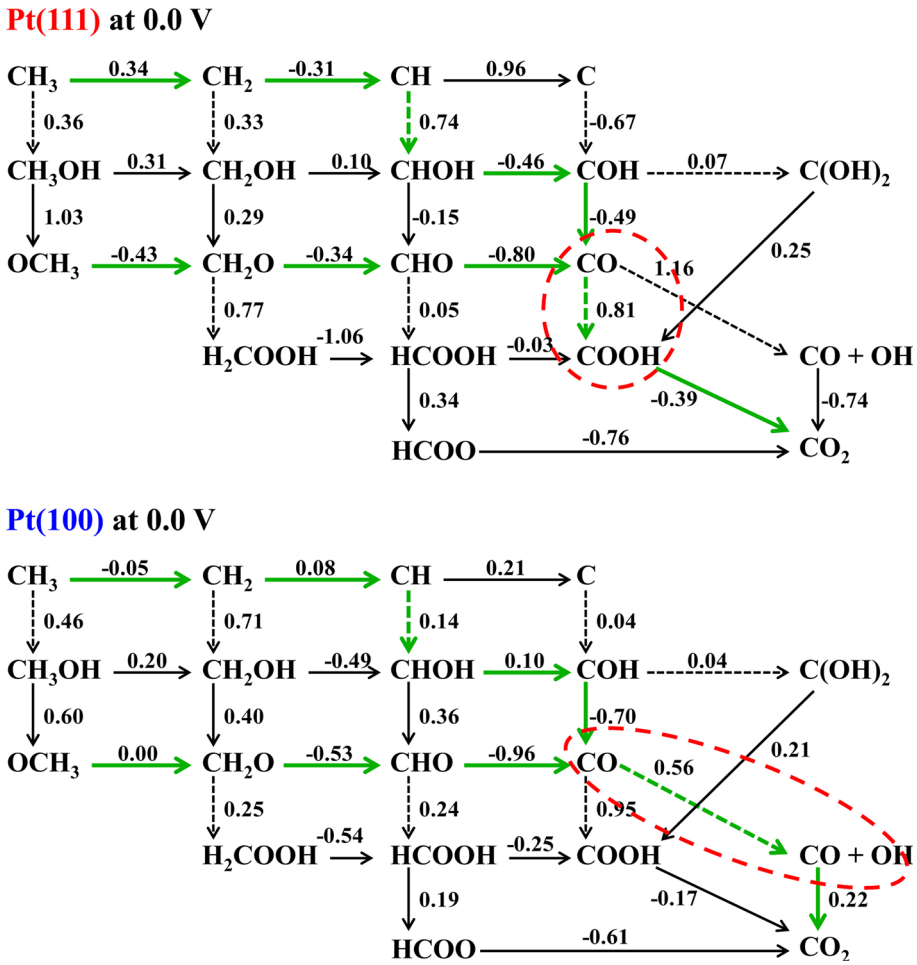

Scheme 4 Electro-oxidation network for C–O bond breaking products of DME on Pt(111) and Pt(100). Values presented are free energies of reaction at 0 V. Stoichiometry is balanced with H_2O, H^+ and e^-. In *dotted arrows* are Heyrovsky type reactions, in *black arrows* are proton/electron transfer reactions. In *green arrows*, the most exergonic pathway is outlined. The *red dashed circle* highlights the most difficult elementary step in the reaction pathways

most difficult part of the oxidation pathway for both surfaces. On Pt(111) it is most favorable to form a COOH species, while on Pt(100) this state is avoided. This is a consequence of the stronger OH binding on Pt(100) than on Pt(111). For Pt(111) CO removal is 0.81 eV endergonic, while it is only 0.56 eV endergonic (the energy required to form adsorbed OH) on Pt(100). Also, CH removal is facile on Pt(100) ($\Delta G = 0.14$ eV), while it is quite difficult on Pt(111) ($\Delta G = 0.74$ eV). Therefore, CH poisoning will not be a problem on Pt(100). Pt(100) should be more active than Pt(111) for these two reasons: (1) more facile CO oxidation, and (2) no CH poisoning.

Now, we consider how the electrode potential will affect this result. From our earlier analysis of C–O bond breaking, we showed that as the potential increases, C–O bond breaking will occur after partial dehydrogenation of DME to some CH_xOCH_y species. When the C–O bond in this species breaks, the CH_x and OCH_y fragments will be oxidized to CO_2. Since the oxidation of these fragments to CO_2 involves only electrochemical steps, the change in the energetics of these steps with potential is uniform. Therefore, if we assumed that CH_3 and OCH_3 were the dissociation products (i.e. no dehydrogenation of DME prior to breaking the C–O bond), then the oxidation pathway would be unchanged and the most difficult steps would still be as previously discussed. However, if different CH_x and OCH_y species are formed, this could change the pathway and most difficult step.

Previously we predicted the oxidation pathway of CH_3 on Pt(111) as: $CH_3 \rightarrow CH_2 \rightarrow CH \rightarrow CHOH \rightarrow COH \rightarrow CO \rightarrow COOH \rightarrow CO_2$. The most difficult step is $CO \rightarrow COOH$. On Pt(100), the predicted pathway is: $CH_3 \rightarrow CH_2 \rightarrow CH \rightarrow CHOH \rightarrow COH \rightarrow CO \rightarrow CO + OH \rightarrow CO_2$. The most difficult step is $H_2O \rightarrow OH$. For CH_x, where $x = 1$ or 2, the same pathway would be found (albeit truncated) because CH_2 and CH are already included in the pathway for CH_3. However, if C were a dissociation product, it can be oxidized on Pt(111) and Pt(100) as $C \rightarrow COH \rightarrow C(OH)_2 \rightarrow COOH \rightarrow CO_2$. Of these, the most difficult elementary step on both Pt(111) and Pt(100) is $C(OH)_2 \rightarrow COOH$, with $\Delta G_{Pt(111)} = 0.25$ eV and $\Delta G_{Pt(100)} = 0.21$ eV. This is significantly easier than the other pathways. However, is it favorable to form C as a dissociation product? C is a possible C–O bond scission product from $COCH_3$, $COCH_2$, COCH, and COC. Of these, C is only a favorable

product from COC (where it must be a product). On the others, it is much more favorable to break the C–O bond to produce CO + CH_x instead of C + OCH_x. From the results shown in Fig. 1, dehydrogenation of DME to COC is only possible at very positive potentials, above 1.07 V on Pt(111) and above 1.13 V on Pt(100). These potentials are above the predicted onset potentials for Pt(111) and Pt(100), so the benefit gained by providing an easier C oxidation route is not practically relevant.

For the OCH_y fragment, the analysis on Pt(111) and Pt(100) is simpler. The predicted oxidation pathway at 0 V on Pt(111) is: $OCH_3 \rightarrow CH_2O \rightarrow CHO \rightarrow CO \rightarrow COOH \rightarrow CO_2$. Again, the most difficult step is CO → COOH. On Pt(100) the pathway is: $OCH_3 \rightarrow CH_2O \rightarrow CHO \rightarrow CO \rightarrow CO + OH \rightarrow CO_2$. The most difficult step is $H_2O \rightarrow OH$, an intermediate step in CO oxidation. Importantly, all possible OCH_y (OCH_3, CH_2O, CHO, and CO) fragments are included in these pathways, and oxidation of CO, the most dehydrogenated species, is the most difficult step. Therefore, whether OCH_3, CH_2O, or CHO or CO are formed via C–O bond breaking, the most difficult step in the pathway does not change.

Overall, the results of our analysis of DME electro-oxidation on Pt(111) and Pt(100) suggest that Pt(100) is more active for two main reasons: (1) At potentials less than 0.99 V (this includes the experimental oxidation potential), C–O bond breaking is easier on Pt(100) than on Pt(111). This is mostly due to C–O bond breaking reaction energetics, which become more exergonic as DME becomes more dehydrogenated. Also, when comparing the surfaces at the same potential, DME can be dehydrogenated to a greater extent on Pt(100) than on Pt(111), Or, DME can be dehydrogenated to the same extent on both surfaces at a lower potential on Pt(100) than on Pt(111). We note that when comparing a single C–O bond breaking step on both surfaces, it is not a general trend that the reaction energy is more exergonic on the (100) surface. (2) The oxidation of the surface poisoning CO is easier on Pt(100), and CH is not a poison on this surface.

3.3 Trends Across (111) and (100) Surfaces

In the previous sections, we described in detail how we analyze the reaction network for DME electro-oxidation on Pt(111) and Pt(100). The main result of our analysis showed that Pt(100) is more active than Pt(111), in agreement with experiments [14–16, 18]. Here, we extend this same analysis to the (111) and (100) facets of Au, Ag, Cu, Pd, Ni, Ir, and Rh to assess if the structure sensitivity results on Pt are general. The free energies of the intermediates adsorbed on these surfaces are shown in Table 1. The analyses of the reaction networks of these surfaces were performed as explained in Sects. 3.1 and 3.2. We note that the corresponding reaction energies (analogous to those shown in Scheme 2 and Scheme 4) are presented in full in the supplemental information.

First, we examine the structure sensitivity of C–O bond breaking on these surfaces. On Pt, we found that eleven of the sixteen C–O bond breaking elementary steps are more exergonic on Pt(100) than on Pt(111). For each of the rest metals we studied, the majority of the C–O bond breaking steps were more exergonic on the (100) facet when compared to the (111) facet. Specifically, we find for Au 10/16, Ag 10/16, Cu 12/16, Pd 12/16, Ni 10/16, Ir 16/16, and Rh 15/16 of the C–O bond breaking steps are more exergonic on the (100) facet (see Table 2 for reaction energies). Again, we cannot conclude any general trend that individual C–O bond breaking steps are always more facile on the (100) facet when compared to the (111) facet of these metals.

Though our results show that most, but certainly not all, C–O bond breaking steps are more facile on the (100) facets of these metals, this result does not necessarily mean that C–O bond breaking of DME will be easier under electrochemical conditions. On Pt, we demonstrated that as DME becomes increasingly dehydrogenated, the reaction energy for breaking the C–O bond in the dehydrogenated species becomes increasingly exergonic. We observe a similar result for all the other metal surfaces in our study. Furthermore, at a particular potential, DME can be dehydrogenated to a greater extent on Pt(100) than on Pt(111) (see Fig. 1). This, in conjunction with more exergonic C–O bond breaking steps (for the majority of C–O bond breaking steps), made C–O bond breaking easier on Pt(100) than Pt(111). We have examined C–O bond breaking as a function of potential from 0 to 1.2 V (see analogous plots to Fig. 1 for other metals in supplemental information). For Au, Ag, Cu, Pd, Ir, and Rh (all metals studied except Ni), C–O bond breaking is more exergonic on the (100) facet over this entire potential range, though the degree to which it is enhanced varies. For example, Pd(100) is calculated to be more active for C–O bond breaking than Pd(111), but the difference in energetics between the two facets is much smaller than for Pt (see SI). C–O bond breaking is more exergonic on Ni(100) than Ni(111) over this range except from 0.71 to 0.90 V. From these results, we conclude that for the metals studied, breaking the C–O bond in DME is more facile on the (100) facet than on the (111).

Though C–O bond breaking is more facile on the (100) facets of these metals, the oxidation of the resultant CH_x and OCH_y (or CH_xO and CH_y) fragments may not be easier on the (100) facet. Following the same approach as on Pt, we calculate the oxidation pathway on these additional metal surfaces and determine the most difficult electro-oxidation step. The corresponding onset potential calculated based on these most difficult steps are plotted for each

Table 2 Free energies of reaction for C–O bond breaking elementary steps on (111) and (100) facets of elemental fcc metals

Elementary step	Free energies of reaction (eV)															
	Au		Ag		Cu		Pt		Pd		Ni		Ir		Rh	
	(111)	(100)	(111)	(100)	(111)	(100)	(111)	(100)	(111)	(100)	(111)	(100)	(111)	(100)	(111)	(100)
$CH_3OCH_3 \rightarrow CH_3 + OCH_3$	1.92	**1.31**	1.38	**1.04**	0.56	**0.23**	0.50	**−0.03**	0.54	**0.51**	−0.27	**−0.45**	0.09	**−0.81**	−0.25	**−0.55**
$CH_2OCH_3 \rightarrow CH_2 + OCH_3$	1.96	**1.17**	1.09	**0.77**	0.17	**0.01**	0.64	**−0.10**	0.46	**0.32**	**−0.72**	−0.65	0.05	**−1.03**	−0.33	**−0.71**
$CH_2OCH_3 \rightarrow CH_3 + CH_2O$	**−0.19**	−0.16	**−0.31**	−0.30	**−0.51**	−0.42	**−0.13**	−0.05	**−0.10**	−0.03	**−0.50**	−0.20	−0.06	**−0.19**	−0.15	**−0.27**
$CHOCH_3 \rightarrow CH + OCH_3$	1.62	**1.43**	1.04	**0.47**	0.05	**−0.64**	0.08	**0.06**	0.18	**−0.02**	−0.74	**−1.22**	−0.33	**−1.22**	−0.71	**−1.15**
$CHOCH_3 \rightarrow CH_3 + CHO$	**−0.31**	−0.12	**−0.04**	0.00	−0.19	**−0.31**	**−0.72**	−0.49	**−0.58**	−0.40	**−0.67**	−0.58	−0.54	**−1.28**	−0.72	**−1.34**
$CH_2OCH_2 \rightarrow CH_2 + CH_2O$	0.16	**−0.07**	**−0.06**	−0.05	**−0.45**	−0.15	0.24	**−0.11**	−0.02	**−0.07**	**−0.67**	0.06	0.05	**0.02**	**−0.11**	0.00
$COCH_3 \rightarrow C + OCH_3$	2.80	**1.88**	2.10	**0.94**	1.49	**0.09**	1.73	**0.49**	1.45	**0.14**	0.74	**−1.38**	0.99	**−0.44**	0.47	**−0.84**
$COCH_3 \rightarrow CH_3 + CO$	−0.84	**−1.17**	−0.99	**−1.13**	**−1.00**	−0.87	−0.81	**−1.24**	**−0.98**	−0.93	−1.04	**−1.55**	−0.82	**−1.19**	−0.85	**−1.27**
$CHOCH_2 \rightarrow CH_2 + CHO$	0.47	**−0.02**	0.57	**0.31**	0.35	**0.11**	0.12	**−0.45**	−0.19	**−0.50**	−0.54	**−0.84**	−0.03	**−1.17**	−0.38	**−1.06**
$CHOCH_2 \rightarrow CH + CH_2O$	0.25	**0.21**	0.26	**−0.29**	−0.09	**−0.65**	**0.15**	0.15	0.02	**−0.47**	−0.38	**−1.03**	0.07	**−0.27**	−0.19	**−0.43**
$COCH_2 \rightarrow C + CH_2O$	**0.21**	0.32	0.26	**−0.35**	−0.35	**−0.60**	0.45	**0.06**	0.22	**−1.07**	0.21	**−0.82**	0.36	**−0.07**	0.18	**−0.70**
$COCH_2 \rightarrow CH_2 + CO$	−1.29	**−1.41**	**−1.43**	−1.34	**−2.16**	−1.12	−1.33	**−1.71**	−1.66	**−1.79**	**−1.79**	−1.44	−1.33	**−1.66**	−1.32	**−1.58**
$CHOCH \rightarrow CH + CHO$	**−0.21**	0.36	**0.18**	0.21	−0.23	**−0.59**	**−0.91**	−0.06	**−1.33**	−0.75	**−1.19**	−0.99	−0.79	**−1.14**	−1.19	**−1.51**
$COCH \rightarrow CH + CO$	**−1.98**	−1.70	**−1.83**	−1.74	−2.05	**−2.51**	**−2.70**	−2.27	−2.72	**−3.08**	−2.79	**−2.92**	−2.34	**−2.43**	−2.34	**−2.66**
$COCH \rightarrow C + CHO$	**−0.27**	−0.21	0.18	**−0.15**	0.20	**−1.22**	−0.94	**−1.10**	−1.06	**−2.39**	−0.95	**−2.11**	−0.74	**−1.75**	−1.04	**−2.41**
$COC \rightarrow C + CO$	−1.20	**−2.07**	−0.20	**−0.59**	−0.90	**−1.80**	−2.81	**−3.19**	−3.03	**−4.37**	−2.23	**−3.83**	−2.69	**−2.95**	−2.57	**−3.49**

For each elementary step on each metal, the facet with the more favorable reaction is indicated with bold font. All species involved are treated as adsorbed to the surface except CH_3OCH_3 and CH_2O, which are gas phase species

surface in Fig. 2. This analysis was performed at 0 V, so the C–O bond is broken in DME, rather than a dehydrogenated species. Therefore, the initial CH_x fragment is CH_3 and the OCH_y fragment is OCH_3 for all surfaces.

The results of our analysis show that complete oxidation of DME to CO_2 is possible at a lower potential on the (100) facet of Au, Ag, Cu, Pt, and Pd than on their (111) facets. On the other hand, a higher potential is required for the (100) facet than the (111) facet of Ni, Ir, and Rh. For Au(111), Ag(111), and Cu(111), the most difficult electrochemical elementary step is the activation of a stable molecule CH_3OH (Au, Ag) or CH_2O (Cu), which are by-products of the oxidation pathway. Since the (100) facets of these metals bind adsorbates stronger than the (111) facets, the activation of these closed-shell species is more exergonic on the (100) facets. As a result, the predicted onset potential for Au(100) and Ag(100) is significantly lower than that on Au(111) and Ag(111), respectively. For Cu, the result is different. Though Cu(111) is limited by activation of a closed-shell species, Cu(100) binds oxygen strongly such that OCH_3 becomes difficult to oxidize. Pt(100) and Pd(100) have lower predicted onset potentials than Pt(111) and Pd(111), respectively, due to more facile CO electro-oxidation. In particular, OH binding is significantly enhanced on the (100) facets which facilitates water activation, thereby producing adsorbed OH species. This OH species is able to oxidize CO without forming a COOH intermediate. For Ni, Ir, and Rh, the (100) facet has a higher onset potential than the corresponding (111) facet. For these metals, the enhanced binding on the more open facet exacerbates surface poisoning. Ni(111) is already limited by removal of strongly bound OCH_3, and this step

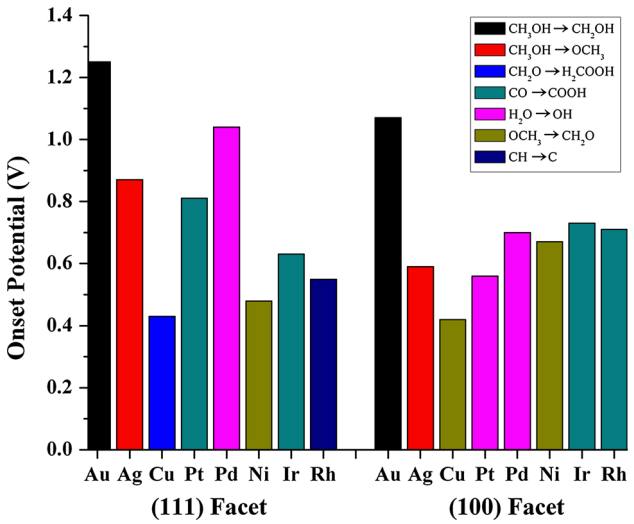

Fig. 2 Calculated onset potential for each surface. The *color* of the *bars* shows the most difficult electrochemical reaction step in the calculated pathway for each surface

becomes even more difficult on Ni(100). Ir(111) binds CO strongly and can be removed either by forming COOH or by directly reacting with coadsorbed OH. However, Ir(100) binds OH too strongly so that only the COOH-mediated pathway is active. In this case, the stronger binding of CO on Ir(100) makes the step more difficult than on Ir(111). On Rh(111), the most difficult electrochemical step is CH oxidation to C, though water activation to remove CO is almost as difficult (preferred over the COOH-mediated pathway). Like Ir(100), on Rh(100) OH binding is too strong, so CO is removed via a COOH-mediated pathway, which is more difficult than on Rh(111).

In the previous analyses, we commented on the difficulty of C–O bond breaking and the onset potential across different fcc metals and their (111)/(100) facets. Each of these provides insight into the relative activity of the different surfaces. To provide a more unified perspective on activity, we have developed theoretical volcano plots [40]. In previous work, we developed volcano plots for DME electro-oxidation on close-packed facets of late transition metals [19]. The volcanos were parameterized with two reactivity descriptors, the free energy of adsorption for CO (G_{CO}) and OH (G_{OH}) and the remainder of the energetics were derived from linear scaling correlations [65]. The specific linear energy correlations were developed from a robust dataset developed for the close packed facets [19]. Here, we have constructed analogous volcano plots at 0.0 V and 0.6 V using linear scaling correlations that were formulated using the data derived for the open facets, as described in Table 1. The (100) volcano plots (Fig. 3c, d) are compared with the respective close-packed facet volcano plots (Fig. 3a, b). The volcano plots present the calculated free energy of reaction for the most endergonic step (i.e. the estimated rate-determining step, ΔG_{RDS}) in the reaction pathway for a hypothetical material with a given value of G_{CO} and G_{OH}, across a range of G_{CO} and G_{OH}. The identity of the rate-determining step within sub-regions of the phase space is indicated in the plots. We caution that this analysis treats the difficulty of C–O bond breaking and electrochemical steps equally [61], while the actual activation energy barriers for the C–O bond breaking events may be quite substantial.

First, we will compare the theoretical volcano plots, and later we will comment on the specific metal surfaces and what ultimately limits their electro-oxidation activity. At first glance, the volcano plots for the close-packed and open facets, at a given potential, are quite similar. That is, comparing Fig. 3a with c, or b with d, the rate-determining step of different regions of the phase-space are similar between the volcanos. Yet, because the specific linear correlations are somewhat different for the two different facets, the slopes and intercepts of the lines separating the sub-regions in the phase space are different. When we

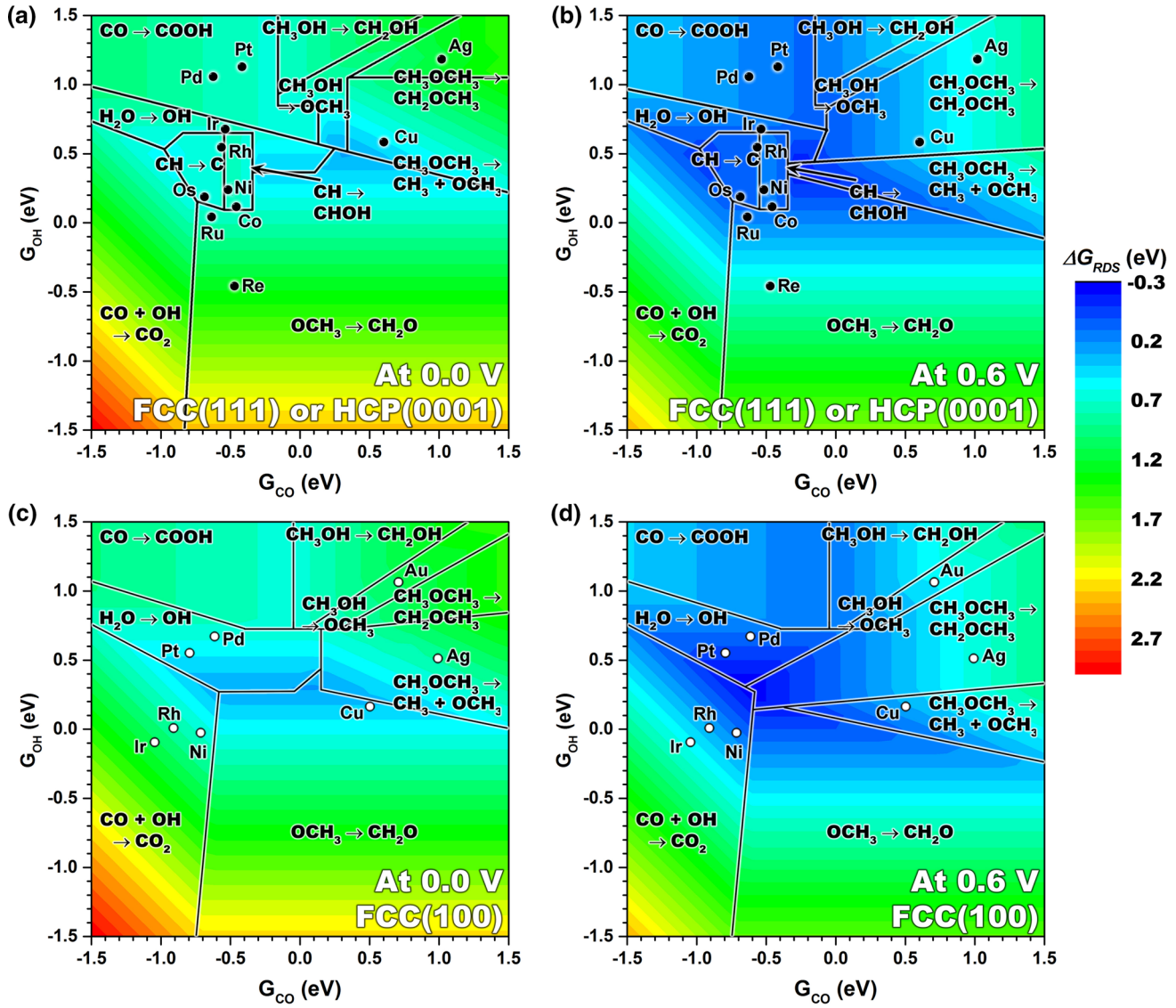

Fig. 3 Theoretical volcano plots generated using linear scaling correlations, derived for **a** close-packed facets at 0.0 V, **b** close-packed facets at 0.6 V, **c** open facets at 0.0 V, and **d** open facets at 0.6 V. Plotted is the free energy of reaction for the most endergonic elementary step in the reaction pathway (ΔG_{RDS}) at the specified potential as a function of the two descriptors, G_{OH} and G_{CO}. The phase space is divided into sub-regions (by *black lines*) by the nature of the most endergonic step (the specific step is described in the figure). The position of specific metal facets, with respect to their G_{OH} and G_{CO} are shown in the plot, though the rigorous DFT-derived ΔG_{RDS} for those materials may differ from the result of the linear scaling correlations. We note that Au(111) is not shown because G_{OH} is outside the phase space, with $G_{OH} = 1.71$ eV and $G_{CO} = 1.19$ eV. The *blue color* represents the region of highest activity, while *red* represents the least active region

compare the optimal binding properties between the different surface structures, we find that the open facet is optimized with stronger CO and OH binding than the close-packed facet.

One important difference between the different facets is that CH poisoning is not a (major) problem on the (100) facets. For the close-packed facets, there is a region of CH poisoning that splits the optimal region in the phase space into two distinct peaks, with the more active peak appearing at a weaker CO adsorption energy than the less active peak; this is more obviously seen at 0.6 V than at 0.0 V. Many of the close-packed facets lie in this region, including Rh(111), Ni(111), Co(0001) and Os(0001). CH is an intermediate in the predicted oxidation pathways on Pt(111), Pd(111), Ir(111), Rh(111), Pt(100), Ir(100), and Rh(100). The free energies of reaction to remove CH at 0.0 V are (from rigorous DFT calculations): 0.74 eV on Pt(111), 0.14 eV on Pt(100), 0.51 eV on Pd(111), −0.22 eV on Pd(100), 0.56 eV on Ir(111), 0.29 eV on Ir(100), 0.55 eV on Rh(111), and −0.06 eV on Rh(100).

For Pt(111), Pd(111), Ir(111), and Rh(111) the electro-oxidation of CH is one of the most difficult steps, of comparable difficulty to CO electro-oxidation. Generally, the (100) facets of these metals preferentially stabilize C with respect to CH, making CH oxidation to C more facile. As a result, CH poisoning is only a problem on the (111) facet of these metals. This finding may have important implications into the observed structure sensitivity of DME electro-oxidation and the preferred facets exposed by the catalytic nanoparticles.

If we compare the change in the volcanos with respect to potential we see similar behavior for both crystal facets. The optimal point in the phase space shifts to stronger CO binding with increased potential, while the optimal OH binding does not change as significantly. The peak shifts with potential because the reaction network has both electrochemical and non-electrochemical elementary steps. As the potential increases, electrochemical reactions become more facile while the energetics for C–O bond breaking are not directly affected. We note that as we described earlier, more facile dehydrogenation (via increased potential) indirectly opens the possibility for a more facile C–O bond breaking event. As a result, with increased potential, the rate-determining step shifts to C–O bond breaking and we can see growth of the sub-regions that are rate-limited by the elementary steps $CH_3OCH_3(g) \rightarrow CH_3 + OCH_3$ and $CH_3OCH_3 \rightarrow CH_2OCH_3$. The latter sub-region tends to consume parts of the former because dehydrogenation of CH_3OCH_3 to CH_2OCH_3 (and further to $COCH_3$) leads to a more facile C–O bond breaking event.

Finally, we comment on how the activity of specific metals changes with respect to their crystal facet. Au(111), Ag(111), Au(100), Ag(100), Cu(111) and Cu(100) bind CO and OH weaker than the optimal substrate for the respective crystal facet. The more open facets of these materials bind CO and OH more strongly than their close-packed facets, and one might assume that this should enhance their activity. However, the optimal binding properties shift to stronger CO and OH binding on the more open facet, which challenges this assumption. Yet, when we ultimately examine the energetics of the rate-determining step, we do predict that Au(100), Ag(100) and Cu(100) are more active than their respective (111) facets. Interestingly, at 0.0 V, Cu(100) is the surface whose binding properties are closest to the optimum, though high activation energy barriers for C–O bond breaking, which are not explicitly accounted for here, may limit the activity of Cu(100). Pt(111) and Pd(111) bind OH too weakly and CO too strongly with respect to the optimal. Compared to their (111) facets, the binding of CO is slightly enhanced on Pt(100) and slightly weakened on Pd(100), while the binding of OH is strongly enhanced on both Pd(100) and Pt(100). These (100) energetics are markedly improved versus their respective close-packed facets, especially at 0.6 V where Pt(100) is the surface which comes closest to the optimum binding. Rh(111) and Ir(111) are similar to Pt and Pd, in that they bind CO too strongly and OH too weakly and they exist in the region of the phase space where CH poisoning is a major problem. Unfortunately, Rh(100) and Ir(100) bind CO and OH much more strongly than the (111) facet of these two metals, and they move further away from the optimal material for (100) facets. Ni behaves similarly, though the OH binding on the (111) facet is already slightly stronger than the optimal value.

Overall, when we consider the onset potential, C–O bond breaking energetics and the volcano analysis, the most promising metal surfaces appear to be Pt(100), Pd(100), and Cu(100). Of these, Cu(100) has the lowest onset potential, but its activity may be limited by C–O bond breaking energetics. Already, experiments and theory [62] have suggested that C–O bond breaking is rate-limiting on Pt(100), and the thermochemistry is even less favorable on Cu(100). Pd(100) has a higher onset potential than Pt(100), and the energetics for C–O bond breaking are also less favorable. Therefore, we suggest that Pt(100) should be the best of the surfaces studied here.

4 Conclusions

We have examined the electro-oxidation of dimethyl ether on the (111) and (100) facets of eight elemental fcc metals. The goal of our study is to explain the experimentally observed structure sensitivity for this reaction on Pt, and to predict how this structure sensitivity would manifest on the other seven metals studied. Our results suggest that Pt(100) is more active than Pt(111) for two main reasons: (1) C–O bond activation is easier on Pt(100) than Pt(111) and (2) the oxidation (i.e. removal) of surface poisons CO and CH that are formed after C–O bond breaking is also easier on Pt(100) than Pt(111). In general, for all metal surfaces studied, breaking the C–O bond in DME (or dehydrogenated DME) is more favorable on the (100) facet because dehydrogenation of DME is more facile on the open facets: in particular, we find that the reaction energy for C–O bond scission in CH_xOCH_y-type species becomes increasingly exergonic as the species becomes increasingly dehydrogenated. As a result, the more facile dehydrogenation on the (100) facet provides more favorable routes to C–O bond activation. In contrast, the oxidation of the C–O bond scission fragments, CH_x and OCH_y, is not always more favorable on the (100) facet. For Au, Ag, Cu, Pt, and Pd, the oxidation of these fragments to CO_2 can occur at a lower potential on the (100) facet, while on Ni, Ir, and Rh, the electro-oxidation of these fragments requires a higher

potential on the (100) facet. The competing C–O bond breaking and CH_x/OCH_y oxidation energetics of the surfaces are simultaneously compared by constructing theoretical volcano plots. From the volcano analysis, we conclude that Au(100), Ag(100), Cu(100), Pt(100), and Pd(100) should be more active than their respective (111) facets, while Ni(100), Rh(100), and Ir(100) will show the opposite trend.

Acknowledgments Prof. Vayenas has inspired many colleagues in the field of electrocatalysis, including these authors. We wish him the best on the occasion of his 65th birthday. This work was supported by DOE-BES, Office of Chemical Sciences. JAH thanks Air Products & Chemicals, Inc. for partial support through a graduate fellowship. Computational work was performed in part using supercomputing resources at the following institutions: EMSL, a National scientific user facility at Pacific Northwest National Laboratory (PNNL); the Center for Nanoscale Materials at Argonne National Laboratory (ANL); and the National Energy Research Scientific Computing Center (NERSC). EMSL is sponsored by the Department of Energy's Office of Biological and Environmental Research located at PNNL. CNM, and NERSC are supported by the U.S. Department of Energy, Office of Science, under contracts DE-AC02-06CH11357, and DE-AC02-05CH11231, respectively.

References

1. Semelsberger TA, Borup RL, Greene HL (2006) Dimethyl ether (DME) as an alternative fuel. J Power Sources 156(2):497–511
2. Floudas CA, Elia JA, Baliban RC (2012) Hybrid and single feedstock energy processes for liquid transportation fuels: a critical review. Comput Chem Eng 41:24–51
3. Serov A, Kwak C (2009) Progress in development of direct dimethyl ether fuel cells. Appl Catal B 91(1–2):1–10
4. Demirci UB (2007) Direct liquid-feed fuel cells: thermodynamic and environmental concerns. J Power Sources 169(2):239–246
5. Yoo JH, Choi HG, Chung CH, Cho SM (2006) Fuel cells using dimethyl ether. J Power Sources 163(1):103–106
6. Yu RH, Choi HG, Cho SM (2005) Performance of direct dimethyl ether fuel cells at low temperature. Electrochem Commun 7(12):1385–1388
7. Kerangueven G, Coutanceau C, Sibert E, Leger JM, Lamy C (2006) Methoxy methane (dimethyl ether) as an alternative fuel for direct fuel cells. J Power Sources 157(1):318–324
8. Kerangueven G, Coutanceau C, Sibert E, Hahn F, Leger JM, Lamy C (2006) Mechanism of di(methyl)ether (DME) electrooxidation at platinum electrodes in acid medium. J Appl Electrochem 36(4):441–448
9. Heinzel A, Barragan VM (1999) A review of the state-of-the-art of the methanol crossover in direct methanol fuel cells. J Power Sources 84(1):70–74
10. Wasmus S, Kuver A (1999) Methanol oxidation and direct methanol fuel cells: a selective review. J Electroanal Chem 461(1–2):14–31
11. Mizutani I, Liu Y, Mitsushima S, Ota KI, Kamiya N (2006) Anode reaction mechanism and crossover in direct dimethyl ether fuel cell. J Power Sources 156(2):183–189
12. Muller JT, Urban PM, Holderich WF, Colbow KM, Zhang J, Wilkinson DP (2000) Electro-oxidation of dimethyl ether in a polymer-electrolyte-membrane fuel cell. J Electrochem Soc 147(11):4058–4060
13. Liu Y, Mitsushima S, Ota K, Kamiya N (2006) Electro-oxidation of dimethyl ether on Pt/C and PtMe/C catalysts in sulfuric acid. Electrochim Acta 51(28):6503–6509
14. Lu LL, Yin GP, Tong YJ, Zhang Y, Gao YZ, Osawa M, Ye S (2008) Electrochemical behaviors of dimethyl ether on platinum single crystal electrodes. Part I: Pt(111). J Electroanal Chem 619:143–151
15. Lu LL, Yin GP, Tong YJ, Zhang Y, Gao YZ, Osawa M, Ye S (2010) Electrochemical behaviors of dimethyl ether on platinum single crystal electrodes. Part II: Pt(100). J Electroanal Chem 642(1):82–91
16. Tong Y, Lu L, Zhang Y, Gao Y, Yin G, Osawa M, Ye S (2007) Surface structure dependent electro-oxidation of dimethyl ether on platinum single-crystal electrodes. J Phys Chem C 111(51):18836–18838
17. Koper MTM (2011) Structure sensitivity and nanoscale effects in electrocatalysis. Nanoscale 3(5):2054–2073
18. Lu LL, Yin GP, Wang ZB, Gao YZ (2009) Electro-oxidation of dimethyl ether on platinum nanocubes with preferential 100 surfaces. Electrochem Commun 11(8):1596–1598
19. Herron JA, Ferrin P, Mavrikakis M (2014) First-principles mechanistic analysis of dimethyl ether electro-oxidation on monometallic single-crystal surfaces. J Phys Chem C 118(42):24199–24211
20. Hammer B, Hansen LB, Nørskov JK (1999) Improved adsorption energetics within density-functional theory using revised Perdew–Burke–Ernzerhof functionals. Phys Rev B 59(11):7413–7421
21. Greeley J, Nørskov JK, Mavrikakis M (2002) Electronic structure and catalysis on metal surfaces. Annu Rev Phys Chem 53:319–348
22. Ferrin P, Mavrikakis M (2009) Structure sensitivity of methanol electrooxidation on transition metals. J Am Chem Soc 131(40): 14381–14389
23. Ferrin P, Nilekar AU, Greeley J, Mavrikakis M, Rossmeisl J (2008) Reactivity descriptors for direct methanol fuel cell anode catalysts. Surf Sci 602(21):3424–3431
24. Greeley J, Mavrikakis M (2002) A first-principles study of methanol decomposition on Pt(111). J Am Chem Soc 124(24): 7193–7201
25. Greeley J, Mavrikakis M (2004) Competitive paths for methanol decomposition on Pt(111). J Am Chem Soc 126(12):3910–3919
26. CRC (2011) Handbook of chemistry and physics, 92nd edn. CRC Press, New York
27. Bengtsson L (1999) Dipole correction for surface supercell calculations. Phys Rev B 59(19):12301–12304
28. Neugebauer J, Scheffler M (1992) Adsorbate-substrate and adsorbate-adsorbate interactions of Na and K adlayers on Al(111). Phys Rev B 46(24):16067–16080
29. Vanderbilt D (1990) Soft self-consistent pseudopotentials in a generalized eigenvalue formalism. Phys Rev B 41(11):7892–7895
30. Chadi DJ, Cohen ML (1973) Special points in Brillouin zone. Phys Rev B 8(12):5747–5753
31. Monkhorst HJ, Pack JD (1976) Special points for Brillouin-zone integrations. Phys Rev B 13(12):5188–5192
32. Perdew JP, Chevary JA, Vosko SH, Jackson KA, Pederson MR, Singh DJ, Fiolhais C (1992) Atoms, molecules, solids, and surfaces—applications of the generalized gradient approximation for exchange and correlation. Phys Rev B 46(11):6671–6687
33. Greeley J, Mavrikakis M (2003) A first-principles study of surface and subsurface H on and in Ni(111): diffusional properties and coverage-dependent behavior. Surf Sci 540(2–3):215–229
34. Rossmeisl J, Qu ZW, Zhu H, Kroes GJ, Nørskov JK (2007) Electrolysis of water on oxide surfaces. J Electroanal Chem 607(1–2):83–89
35. Rossmeisl J, Logadottir A, Nørskov JK (2005) Electrolysis of water on (oxidized) metal surfaces. Chem Phys 319(1–3):178–184
36. Karlberg GS, Rossmeisl J, Nørskov JK (2007) Estimations of electric field effects on the oxygen reduction reaction based on

the density functional theory. Phys Chem Chem Phys 9(37): 5158–5161
37. Nørskov JK, Rossmeisl J, Logadottir A, Lindqvist L, Kitchin JR, Bligaard T, Jonsson H (2004) Origin of the overpotential for oxygen reduction at a fuel-cell cathode. J Phys Chem B 108(46):17886–17892
38. Herron JA, Ferrin P, Mavrikakis M (2015) Electrocatalytic oxidation of ammonia on transition-metal surfaces: a first-principles study. J Phys Chem C 119(26):14692–14701
39. Logadottir A, Rod TH, Nørskov JK, Hammer B, Dahl S, Jacobsen CJH (2001) The Bronsted–Evans–Polanyi relation and the volcano plot for ammonia synthesis over transition metal catalysts. J Catal 197(2):229–231
40. Nørskov JK, Bligaard T, Logadottir A, Bahn S, Hansen LB, Bollinger M, Bengaard H, Hammer B, Sljivancanin Z, Mavrikakis M, Xu Y, Dahl S, Jacobsen CJH (2002) Universality in heterogeneous catalysis. J Catal 209(2):275–278
41. Ojeda M, Nabar R, Nilekar AU, Ishikawa A, Mavrikakis M, Iglesia E (2010) CO activation pathways and the mechanism of Fischer–Tropsch synthesis. J Catal 272(2):287–297
42. Grabow LC, Hvolbaek B, Nørskov JK (2010) Understanding trends in catalytic activity: the effect of adsorbate–adsorbate interactions for CO oxidation over transition metals. Top Catal 53(5–6):298–310
43. Miller SD, Inoglu N, Kitchin JR (2011) Configurational correlations in the coverage dependent adsorption energies of oxygen atoms on late transition metal fcc(111) surfaces. J Chem Phys 134(10):104709
44. Wu C, Schmidt DJ, Wolverton C, Schneider WF (2012) Accurate coverage-dependence incorporated into first-principles kinetic models: catalytic NO oxidation on Pt (111). J Catal 286:88–94
45. Getman RB, Xu Y, Schneider WF (2008) Thermodynamics of environment-dependent oxygen chemisorption on Pt(111). J Phys Chem C 112(26):9559–9572
46. Desai S, Neurock M (2003) A first principles analysis of CO oxidation over Pt and Pt66.7%Ru33.3% (111) surfaces. Electrochim Acta 48(25–26):3759–3773
47. Koper MTM (2005) Combining experiment and theory for understanding electrocatalysis. J Electroanal Chem 574(2):375–386
48. Lew WD, Crowe MC, Karp E, Campbell CT (2011) Energy of molecularly adsorbed water on clean Pt(111) and Pt(111) with coadsorbed oxygen by calorimetry. J Phys Chem C 115(18): 9164–9170
49. Ogasawara H, Brena B, Nordlund D, Nyberg M, Pelmenschikov A, Pettersson LGM, Nilsson A (2002) Structure and bonding of water on Pt(111). Phys Rev Lett 89(27):276102
50. Rossmeisl J, Greeley J, Karlberg GS (2008) Electrocatalysis and catalyst screening from density functional theory calculations. In: Koper MTM (ed) Fuel cell catalysis: a surface science approach. Wiley, Hoboken
51. Mistry H, Reske R, Zeng ZH, Zhao ZJ, Greeley J, Strasser P, Cuenya BR (2014) Exceptional size-dependent activity enhancement in the electroreduction of CO_2 over Au nanoparticles. J Am Chem Soc 136(47):16473–16476
52. Karamad M, Tripkovic V, Rossmeisl J (2014) Intermetallic alloys as CO electroreduction catalysts—role of isolated active sites. ACS Catal 4(7):2268–2273
53. Van Santen RA (2009) Complementary structure sensitive and insensitive catalytic relationships. Acc Chem Res 42(1):57–66
54. Ciobica IM, van Santen RA (2003) Carbon monoxide dissociation on planar and stepped Ru(0001) surfaces. J Phys Chem B 107(16):3808–3812
55. Andersson MP, Abild-Pedersen E, Remediakis IN, Bligaard T, Jones G, Engbwk J, Lytken O, Horch S, Nielsen JH, Sehested J, Rostrup-Nielsen JR, Nørskov JK, Chorkendorff I (2008) Structure sensitivity of the methanation reaction: H_2-induced CO dissociation on nickel surfaces. J Catal 255(1):6–19
56. Dahl S, Logadottir A, Egeberg RC, Larsen JH, Chorkendorff I, Tornqvist E, Nørskov JK (1999) Role of steps in N_2 activation on Ru(0001). Phys Rev Lett 83(9):1814–1817
57. Spencer ND, Schoonmaker RC, Somorjai GA (1982) Iron single-crystals as ammonia-synthesis catalysts—effect of surface-structure on catalyst activity. J Catal 74(1):129–135
58. Loffreda D, Simon D, Sautet P (2003) Structure sensitivity for NO dissociation on palladium and rhodium surfaces. J Catal 213(2):211–225
59. Ge Q, Neurock M (2004) Structure dependence of NO adsorption and dissociation on platinum surfaces. J Am Chem Soc 126(5):1551–1559
60. Liu ZP, Hu P (2003) General rules for predicting where a catalytic reaction should occur on metal surfaces: a density functional theory study of C-H and C–O bond breaking/making on flat, stepped, and kinked metal surfaces. J Am Chem Soc 125(7):1958–1967
61. Koper MTM (2011) Thermodynamic theory of multi-electron transfer reactions: implications for electrocatalysis. J Electroanal Chem 660(2):254–260
62. Li HJ, Calle-Vallejo F, Kolb MJ, Kwon Y, Li YD, Koper MTM (2013) Why (100) terraces break and make bonds: oxidation of dimethyl ether on platinum single-crystal electrodes. J Am Chem Soc 135(38):14329–14338
63. Li HJ, Li YD, Koper MTM, Calle-Vallejo F (2014) Bond-making and breaking between carbon, nitrogen, and oxygen in electrocatalysis. J Am Chem Soc 136(44):15694–15701
64. Lebedeva NP, Rodes A, Feliu JM, Koper MTM, van Santen RA (2002) Role of crystalline defects in electrocatalysis: CO adsorption and oxidation on stepped platinum electrodes as studied by in situ infrared spectroscopy. J Phys Chem B 106(38):9863–9872
65. Abild-Pedersen F, Greeley J, Studt F, Rossmeisl J, Munter TR, Moses PG, Skulason E, Bligaard T, Nørskov JK (2007) Scaling properties of adsorption energies for hydrogen-containing molecules on transition-metal surfaces. Phys Rev Lett 99(1):016105